Signal Transduction

Molecular Cancer Research

Exosomal Annexin II Promotes Angiogenesis and Breast Cancer Metastasis

Sayantan Maji[1,2], Pankaj Chaudhary[1,2], Irina Akopova[3], Phung M. Nguyen[3], Richard J. Hare[4], Ignacy Gryczynski[3], and Jamboor K. Vishwanatha[1,2,5]

Abstract

Tumor-derived exosomes are emerging mediators of tumorigenesis and tissue-specific metastasis. Proteomic profiling has identified Annexin II as one of the most highly expressed proteins in exosomes; however, studies focused on the biological role of exosomal Annexin II (exo-Anx II) are still lacking. In this study, mechanistic insight was sought regarding exo-Anx II and its function in angiogenesis and breast cancer metastasis. Multiple *in vitro* and *in vivo* techniques were used to study the role of exo-Anx II in angiogenesis. Using atomic force microscopy and Western blotting, exo-Anx II expression was characterized in normal and breast cancer cells. In addition, organ-specific metastatic breast cancer cells and animal models were used to define the role exo-Anx II in breast cancer metastasis. Results revealed that exo-Anx II expression is significantly higher in malignant cells than normal and premetastatic breast cancer cells. *In vitro* and *in vivo* studies demonstrated that exo-Anx II promotes tPA-dependent angiogenesis. Furthermore, *in vivo* analysis indicated that metastatic exosomes create a favorable microenvironment for metastasis, and exo-Anx II plays an important role in this process, as priming with Anx II-depleted exosomes reduces brain (∼4-fold) and lung (∼2-fold) metastasis. Upon delineating the mechanism, it was discovered that exo-Anx II causes macrophage-mediated activation of the p38MAPK, NF-κB, and STAT3 pathways and increased secretion of IL6 and TNFα. These data demonstrate an important role for exo-Anx II in breast cancer pathogenesis.

Implications: Exosome-associated Annexin II plays an important role in angiogenesis and breast cancer metastasis, which can be exploited as a potential biomarker as well as a therapeutic target for diagnosis and treatment of metastatic breast cancer. *Mol Cancer Res; 15(1); 93–105. ©2016 AACR.*

Introduction

Exosomes are membrane vesicles, 40 to 100 nm in diameter, secreted from almost all cell types under both physiologic and pathologic conditions. Tumor-derived exosomes possess immunosuppressive properties and can facilitate tumor growth, metastasis, and the development of drug resistance, effects that can contribute to cancer pathogenesis. By stimulating angiogenesis (1), modulating stromal cells, and remodeling extracellular matrix (ECM; 2, 3), tumor-derived exosomes contribute to the establishment of a premetastatic niche and generate suitable microenvironments in distant metastatic sites (4). Furthermore, recent discoveries have shown that exosomes from gynecologic neoplasias, including ovarian cancer and breast cancer, contain metalloproteinases that have proteolytic activity, which aids in metastasis; thus, exosomes were found to increase the rate of ECM degradation and augment tumor invasion into the stroma (5).

Annexin II (Anx II) is a Ca^{2+}-dependent phospholipid-binding protein associated with the plasma membrane and the endosomal system. Anx II is upregulated in breast cancer and implicated in many cancer-associated functions, including plasminogen activation, actin–cytoskeletal rearrangement (6), cellular migration, adhesion, and proliferation (7). Specifically, increased cell surface expression of Anx II has been shown to contribute to increased angiogenesis and ECM degradation (7, 8). Anx II acts as a coreceptor for tissue plasminogen activator (tPA) and plasminogen, which can form heterotetrameric complexes on the surfaces of cells with the Anx II light chain, S100A10 or p11, and this stimulates the generation of tPA-dependent plasmin. Plasmin is a highly reactive enzyme that is physiologically involved in fibrinolysis and plays an important role in neoangiogenesis (8–10). Previously, it has been shown that Anx II is associated with the lipid rafts and influenced by intracellular Ca^{2+} levels and N-terminal phosphorylation at tyrosine-23 (11). We have previously shown that binding of Anx II to the lipid rafts is followed by its transport along the endocytic pathway to be associated with the intraluminal vesicles of the multivesicular endosomes. Anx II-containing multivesicular endosomes then fuse directly with the plasma membrane, resulting in the release of the intraluminal vesicles into the extracellular environment, facilitating the exogenous transfer of Anx II from one cell to another, a novel pathway of extracellular transport of Anx II (11).

Proteomic profiling data from ExoCarta (12) have indicated that Anx II is abundant in the exosomes. In addition, secreted Anx II levels have been shown to positively correlate with the

[1]Department of Molecular and Medical Genetics, University of North Texas Health Science Center, Fort Worth, Texas. [2]Institute for Cancer Research, University of North Texas Health Science Center, Fort Worth, Texas. [3]Department of Cell Biology and Immunology, University of North Texas Health Science Center, Fort Worth, Texas. [4]Plaza Medical Center of Fort Worth, Fort Worth, Texas. [5]Texas Center for Health Disparities, University of North Texas Health Science Center, Fort Worth, Texas.

Note: Supplementary data for this article are available at Molecular Cancer Research Online (http://mcr.aacrjournals.org/).

Current address for S. Maji: Mayo Clinic, 4500 San Pablo Rd, Jacksonville, FL.

Corresponding Author: Sayantan Maji, University of North Texas Health Science Center, 3500 Camp Bowie Blvd, EAD 248, Fort Worth, TX 76107. Phone: 817-735-0494, Fax: 817-735-0695; E-mail: sayantan.maji@live.unthsc.edu

doi: 10.1158/1541-7786.MCR-16-0163

invasiveness of breast cancer cells (13); however, to the best of our knowledge, no study has explored the biological role of exosomal Anx II (exo-Anx II), especially in cancer. In the current study, we characterized exo-Anx II in a breast cancer progression model. In addition, using Anx II competitive inhibitory peptide LCKLSL (14, 15) as well as shRNA-mediated knockdown of Anx II, we showed that exo-Anx II promotes angiogenesis and organ-specific metastasis, two of the key hallmarks of cancer.

Materials and Methods

Cell line models

For the comparative analysis of exo-Anx II, a MCF10A progression model (received as a gift from Dr. Judith Christman, University of Nebraska Medical Center, Omaha, NE) was used: MCF10A (nonmalignant), MCF10AT (premalignant), and MCF10CA1a (malignant). For the metastasis studies, MDA-MB-231 (ATCC) and its organ-specific metastatic variants [received as a gift from Dr. Joan Massagué, Memorial Sloan Kettering Cancer Center (New York City, NY) and shipped by the Antibody and Bioresource Core Facility] were used: MDA-MB-831 (brain metastasis) and MDA-MB-4175 (lung metastasis). The cell lines were authenticated by performing STR analysis with the Promega PowerPlex Fusion V1.0. All the cells tested negative for mycoplasma infection when tested with MycoAlert PLUS from Lonza. The cell lines were not reauthenticated by the authors.

Cell culture

MCF10A cells were cultured as described in ref. 14, MCF10AT and MCF10CA1a cells were cultured as described in ref. 16, and MDA-MB-231, MDA-MB-831, and MDA-MB-4175 cells were cultured as described in ref. 17. Pooled Clonetics Human Umbilical Vein Endothelial Cells (HUVEC; Lonza) were grown in EGM Media plus bovine brain extract at 37°C in 5% CO_2.

Antibodies and reagents

The following antibodies were used: anti-Anx II (BD Biosciences), anti-GAPDH, anti-CD81, anti-Arginase 1 (Santa Cruz Biotechnology), anti-phospho-p38 (Thr180/Tyr182), anti-p38, anti-phospho-NF-κB p65 (S536), anti-NF-κB p65, anti-phospho-STAT-3 (Y705), anti-STAT-3, anti-MMP9, anti-VEGF (Cell Signaling Technology), anti-human vimentin (NCL-L-VIM-V9, Leica Biosystems), anti-mouse CD31, anti-tPA, anti-VEGFR1 (Abcam), anti-calnexin (Enzo), anti-CD63 (Developmental Studies Hybridoma Bank, University of Iowa, Iowa City, IA), anti-uPA (R&D Systems), anti-F4/80 (AbD Serotec), and 25-nm gold nanoparticle-tagged secondary anti-mouse antibody (Electron Microscopy Sciences). We also used protein A/G beads for immunoprecipitation (IP; Santa Cruz Biotechnology), Versene (Gibco, Thermo Fisher Scientific), India ink dye (American Master Tech), Calcein-AM dye (Life Technologies, Thermo Fisher Scientific), PKH26 (Sigma-Aldrich), Matrigel and Matrigel-HC (BD Biosciences), D-luciferin (Caliper Life Sciences), LCKLSL and LGKLSL peptides (Bio Basic Inc.), and a mouse TNFα and IL6 ELISA Kit (eBioscience).

Exosome isolation and characterization

Exosomes were isolated by ultracentrifugation (18) and labeled with PKH26 (Sigma-Aldrich), as described previously (19). Secreted exosomes were quantified by measuring acetylcholinesterase activity (15). Electron microscopy (18) and atomic force microscopy (20) of the exosomes were performed as published previously.

Migration, invasion, and angiogenesis assay

Migration and invasion assays were performed with BD Transwell invasion assay inserts, according to the manufacturer's protocol. The Matrigel plug assay was performed as described previously (21). Briefly, 400 μL of Matrigel (~20 mg/mL) was injected subcutaneously, along with PBS, VEGF, or different exosome treatments with or without the peptides. After 12 days, the Matrigel plugs were isolated and imaged. Half of the plugs were processed for immunohistologic analysis, and half were used for hemoglobin estimation by Drabkin's method, using a previously published protocol (22, 23). For all these assays, we used LCKLSL inhibitory or LGKLSL control peptides as published previously (14, 15).

shRNA-mediated downregulation of Anx II

To downregulate exo-Anx II, shRNA against Anx II (GIPZ Lentiviral Human ANXA2 and shRNA, GE Dharmacon) was used. Exosomes isolated from shAnx II and shControl cells were designated as Anx IIKD-Exo and Control-Exo, respectively.

Animal studies

The animals were procured under Institutional Animal Care and Use Committee (IACUC)-approved protocols, and all the studies and experiments were carried out in accordance with the IACUC protocol for animal handling. Four- to 6-week-old female athymic nude mice (Harlan Laboratories) were used for all the animal studies.

Priming of animals with exosomes

To study the role of exo-Anx II in metastasis, the animals were injected with PBS or exosomes from breast cancer cells stably transfected with shControl (Control-Exo) or with sh-Anx II (Anx IIKD-exo). Priming was performed via regular injection of 100 μg of exosomal proteins in 100 μL PBS via the lateral tail vein, twice a week for 4 weeks.

Metastasis models

To check the role of exo-Anx II in promoting breast cancer metastasis, two different models were used: intravenous (lateral tail vein) lung metastasis and an intracardiac metastasis model. MDA-MB-231, MDA-MB-831, and MDA-MB-4175 cells were used for the metastasis study. At the end of exosome priming, the primed animals were challenged with the respective luciferase-positive breast cancer cells, and the difference in the extent of organ-specific metastasis over time was studied via bioluminescence imaging (BLI). At the end of the study, the animals were sacrificed and the organs were harvested and analyzed further by hematoxylin and eosin (H&E) staining and DAB immunostaining (anti-human vimentin) to stain the metastasized human breast cancer cells. Lung and brain sections were also analyzed by a pathologist for the presence or absence of immunostaining in the organ stroma.

Intravenous (tail vein) injection (24, 25) and intracardiac inoculation (26) of luciferase-positive breast cancer cells were performed as published previously.

In vivo imaging of animals

In vivo animal imaging using an IVIS Lumina XR system (Caliper Life Sciences) was performed weekly, as published previously (26). In each study, identical exposure times were used to detect BLI among the different treatment groups.

Histologic analyses of tissues

H&E staining as well as immunohistochemical analyses of paraffin-blocked tissue sections were performed using standard procedures. Respective isotype-matched mouse and rabbit normal IgG antibodies were used as controls for all immunostainings. Furthermore, for IHC, an additional Fc receptor–blocking step was performed to rule out the possibility that exosome treatment increases the expression of Fc gamma receptor, which might nonspecifically bind primary antibodies used in the IHC.

ELISA for IL6 and TNFα

ELISA Kits were purchased from eBioscience, and ELISA was performed according to the manufacturer's protocol.

Immunoprecipitation and signaling

For the IP experiment, 231-Anx IIKD cells were treated with PBS/231-Anx IIKD-exo or 231-Control-Exo (100 μg protein) and returned to the incubator for 6 hours. Next, the cells were washed with PBS, and the membrane proteins were stripped via Versene wash (0.5 mmol/L EDTA and PBS buffer). The Versene eluates were centrifuged at 10,000 × *g* for 15 minutes to remove any cell debris and immunoprecipitated with pro-cathepsin B antibody overnight and probed for Anx II. For the signaling experiments, HUVECs were treated with PBS/231-Anx IIKD-exo or 231-Control-Exo (100 μg protein) and returned to the incubator. After the incubation, the cells were washed, whole-cell lysates (WCL) were collected in NP40 lysis buffer, and Western blotting was performed with the designated antibodies. For tPA studies, HUVECs were pretreated with PBS/tPA antibody (2 μg/mL) or IgG control antibody (2 μg/mL) for 2 hours, followed by treatment with MDA-MB-231 exosomes (100 μg), and kept for 6 hours at 37°C. After incubation, the cells were fixed and photographed. The number of branch points/field and number of meshes/field were counted via NIH ImageJ software to quantify the angiogenic response.

Statistical analysis

Results are expressed as arithmetic means ± SEM if not otherwise indicated. Values of $P \leq 0.05$ were considered statistically significant, as determined by the unpaired Mann–Whitney test, the two-tailed unpaired Student *t* test, or the Wilcoxon signed-rank test, where appropriate. For all the figures, $^{*}P < 0.05$, $^{**}P < 0.01$, $^{***}P < 0.001$, and $^{****}P < 0.0001$. GraphPad Prism statistical software was used for all statistical analyses. NCSS Power analysis software was used for animal studies.

Results

Exo-Anx II correlates positively with the aggressiveness of breast cancer cells

To characterize exo-Anx II expression, we used the MCF10A breast cancer progression model, which consists of MCF10A (immortalized mammary epithelial cell line), MCF10AT (premalignant cell line generated by *HRAS* transformation of MCF10A), and MCF10CA1a (derived from poorly differentiated malignant tumors of MCF10AT xenografts) cells (27). Western blotting of exosomal lysate from MCF10A, MCF10AT, and MCF10CA1a revealed that exo-Anx II levels highly correlated with the aggressiveness of the breast cancer cells, with lower levels in MCF10A, moderate levels in MCF10AT, and significantly higher levels in MCF10CA1a (Fig. 1A); however, WCL analysis of the progression model revealed no significant changes in the levels of Anx II in MCF10AT and MCF10CA1a (Supplementary Fig. S1H). Densitometry revealed that exo-Anx II levels were approximately 5-fold greater in MCF10CA1a exosomes than in MCF10A exosomes (Fig. 1B). Interestingly, the levels of other angiogenic markers, including VEGF, urokinase-type plasminogen activator, and matrix metalloproteinase 9 (MMP9), were relatively unchanged (Supplementary Fig. S1G). CD81 was used as a specific exosomal marker and a loading control.

Expression of exo-Anx II is higher in MCF10CA1a exosomes than MCF10A exosomes

Scanning of exosomes in the MCF10A progression model by atomic force microscope revealed a higher surface expression of Anx II on the MCF10CA1a exosomes than the MCF10A exosomes, as depicted by increased surface binding of 25-nm gold nanoparticle-tagged anti-Anx II antibody (Fig. 1C). Quantification of the number of gold nanoparticles per field revealed almost approximately 5-fold greater binding of gold nanoparticles on MCF10CA1a exosomes than MCF10A exosomes (Fig. 1D). Surface topography analysis confirmed these findings, showing multiple peaks corresponding to higher gold nanoparticle binding in MCF10CA1a exosomes, but much less in MCF10A exosomes after treatment with Anx II antibody (Fig. 1E), indicating that MCF10CA1a exosomes have more Anx II surface expression than MCF10A exosomes. The exosomal marker CD63 and the endoplasmic reticulum marker calnexin served as positive and negative controls, respectively.

Exo-Anx II promotes angiogenesis

As Anx II has been implicated in promoting angiogenesis previously (7, 14, 15), in the current study, we investigated whether exo-Anx II, once secreted from cells, is capable of promoting angiogenesis as well. In an *in vitro* model of angiogenesis, we compared the angiogenic potential of exo-Anx II in MCF10A, MCF10AT, and MCF10CA1a cells using LCKLSL and LGKLSL peptides (14, 15). The *in vitro* endothelial tube formation assay showed that exosome treatments resulted in approximately 4-, 6-, and 7.5-fold increases in the number of meshes per field and approximately 1.4-, 1.8, and 2-fold increases in the number of branch points per field with MCF10A, MCF10AT, and MCF10CA1a exosomes, respectively (Supplementary Fig. S2A and S2C). Interestingly, exosome incubation with LCKLSL nullified the angiogenic effect of exo-Anx II (a ∼3-fold decrease in the number of meshes per field and ∼0.75-fold decrease in the number of branch points per field in the case of MCF10CA1a); however, treatment with LGKLSL had no effect (Supplementary Fig. S2A–S2D). Incubation of LCKLSL with MCF10A and MCF10AT exosomes showed similar effects (data not shown).

Endothelial cell migration and invasion is an important step in angiogenesis (28) and Anx II-p11-tPA–mediated plasmin

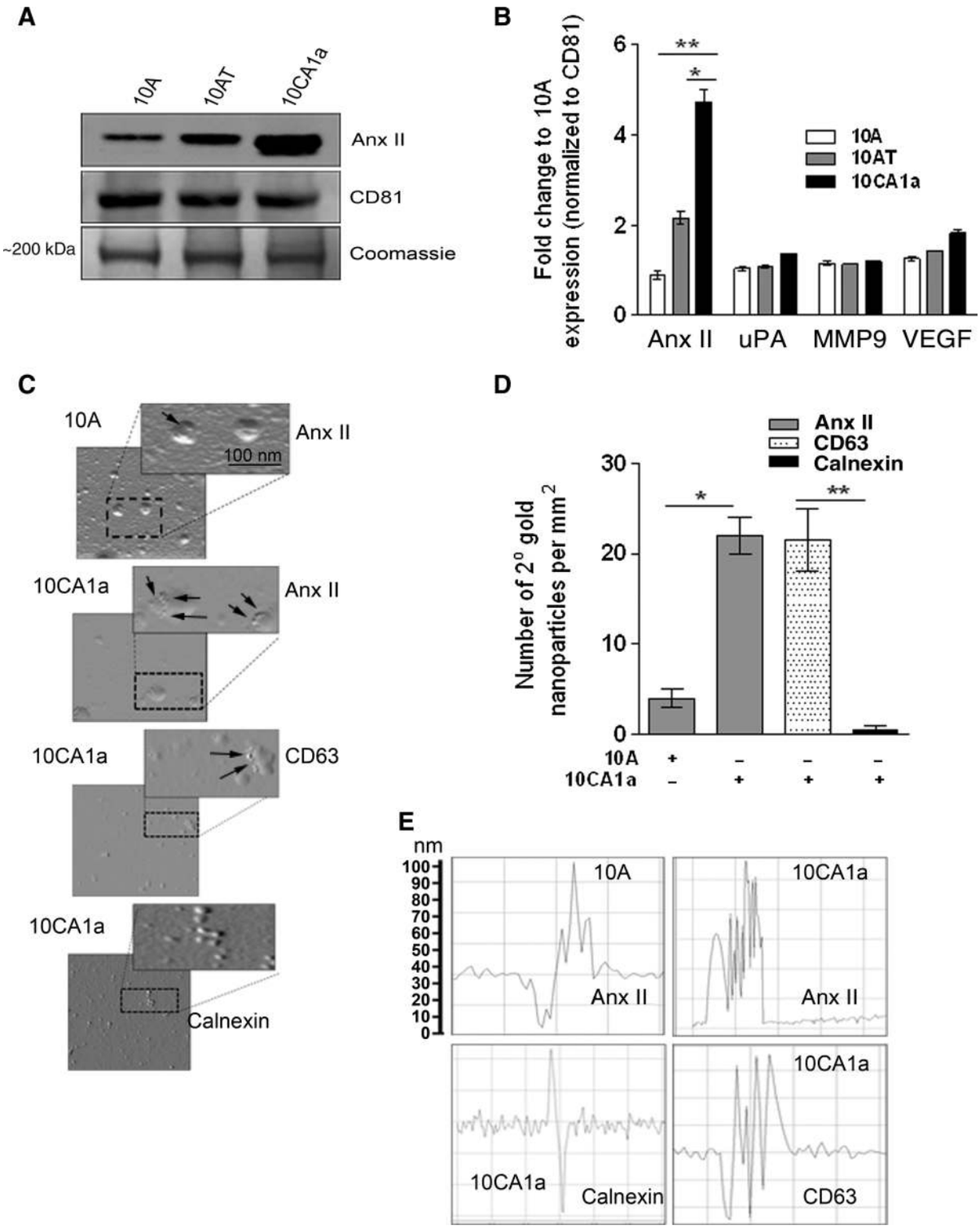

Figure 1.

Characterization of exosomes. **A,** Western blot analysis of the different protein levels in the exosomes collected from the MCF10A-, MCF10AT-, and MCF10CA1a-conditioned media. CD81 was used as a loading control ($n = 3$). The Coomassie band confirms equal loading. **B,** Quantification of the Western blots. Fold change to CD81 is shown. uPA, urokinase-type plasminogen activator. **C,** Atomic force microscopy (AFM) analysis of MCF10A exosomes and MCF10CA1a exosomes. Anx II, calnexin, or CD63 immunoreactivity was identified by 25-nm gold nanoparticles. **D,** Quantification of the AFM data representing the number of secondary (2°) gold nanoparticles per field. Four independent fields were counted. **E,** Surface topology analysis of the exosomes using the AFM NT-MDT software ($n = 2$). *, $P < 0.05$; **, $P < 0.01$.

generation potently promotes this process (7). Thus, to further confirm the role of exo-Anx II in plasmin generation and angiogenesis, we studied the effect of exo-Anx II on the migration and invasion of HUVECs. HUVECs were added with the respective exosomes, with or without LCKLSL or LGKLSL, into the upper chamber of the transwell and incubated for 24 hours. After incubation, the number of cells that migrated to or invaded the other side of the membrane was counted. Treatment with MCF10CA1a exosomes plus LCKLSL led to a significant decrease in both migration (∼40%) and invasion (∼30%) of HUVECs, compared with MCF10CA1a exosome treatment only or with LGKLSL (Supplementary Fig. S1J–S1L).

To confirm our *in vitro* findings and to study the proangiogenic role of exo-Anx II in a physiologically relevant setting, we performed an *in vivo* Matrigel plug assay (21). Mice were injected subcutaneously with Matrigel in the presence of PBS alone (negative control), Matrigel mixed with VEGF (positive control), or Matrigel mixed with respective exosome treatments. The LGKLSL or LCKLSL peptides were incorporated into the Matrigel plugs in the presence of the exosomes. Twelve days after the implantation of Matrigel, the mice were sacrificed and the Matrigel plugs were isolated and imaged for angiogenesis. Half of the plugs were sectioned for immunohistochemical analysis to study blood vessel formation and CD31 (endothelial cell marker) staining. The remaining plugs were homogenized and their hemoglobin content was estimated to quantify angiogenesis.

Analysis of the Matrigel plugs showed that MCF10CA1a exosome treatment induced significantly higher angiogenesis than the MCF10AT and MCF10A exosomes (Fig. 2B). Hemoglobin estimation of the homogenized Matrigel plugs confirmed these results, showing approximately 5-, 14-, and 24-fold

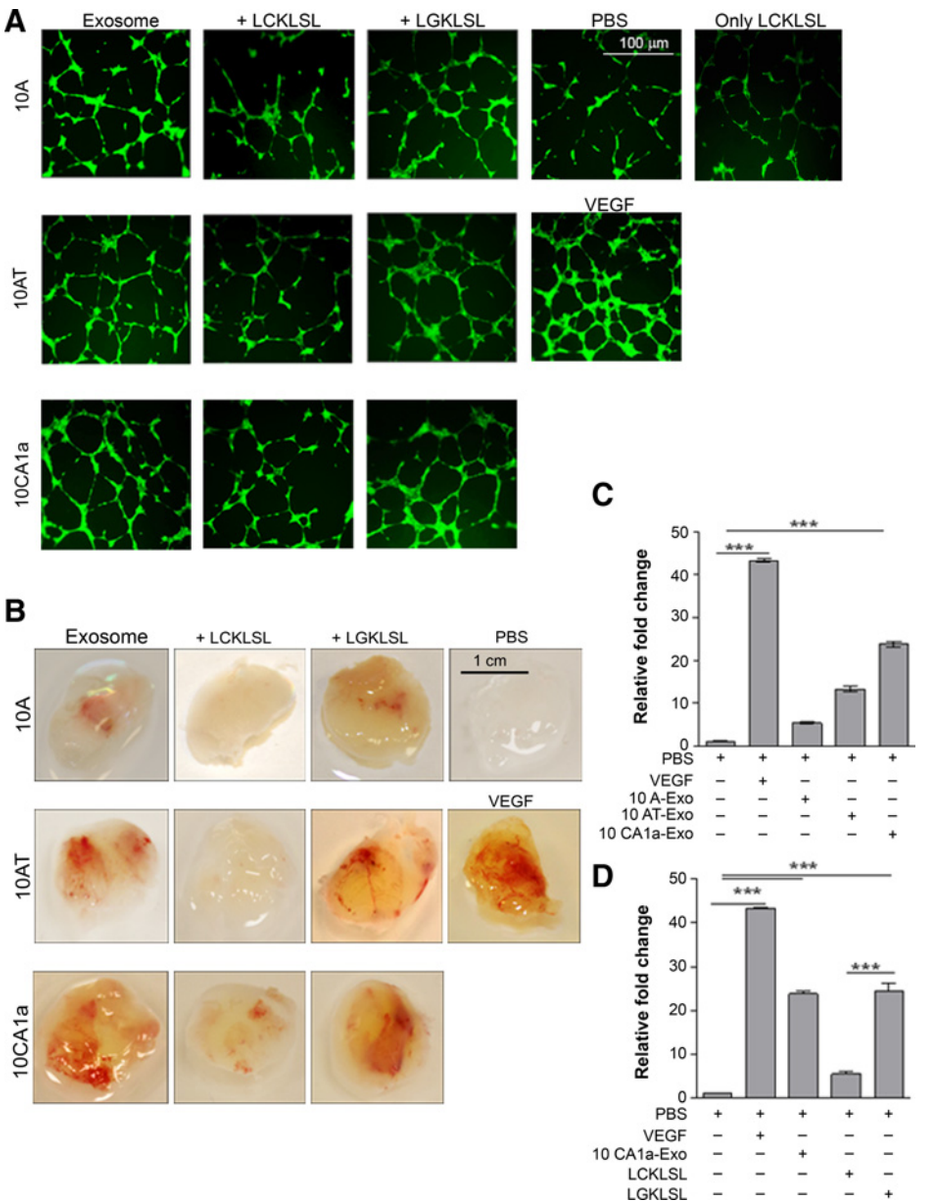

Figure 2.
Exo-Anx II promotes angiogenesis. Effect of exo-Anx II on *in vitro* tube formation assay. **A,** Fluorescent images of *in vitro* endothelial tube formation assay with HUVECs (5 different fields per group were considered; repeated in triplicates). PBS (negative control), VEGF (100 ng/mL, positive control), and 100 μg of exosomal proteins were used ($n = 3$). Peptide concentration used: 5 μmol/L ($n = 3$). Exosomes from MCF10A, MCF10AT, and MCF10CA1a cells are designated as 10A, 10AT, and 10CA1a, respectively. Scale bar, 100 μm. Matrigel plug assay: mice were injected with Matrigel in the presence of PBS alone (negative control), VEGF alone (100 ng/mL, positive control), or 100 μg exosomes ± peptide. After 12 days, the plugs were removed and the angiogenic responses were evaluated. **B,** Representative images of Matrigel plugs are shown. Scale bar, 1 cm. **C** and **D,** Hemoglobin estimation of homogenized Matrigel plugs by Drabkin's method. Fold change to PBS is shown. Peptide concentration: 5 μmol/L ($n = 3$). Exosomes from MCF10A, MCF10AT, and MCF10CA1a cells are designated as 10A, 10AT, and 10CA1a, respectively. ***, $P < 0.001$.

increases in the hemoglobin content when incubated with MCF10A, MCF10AT, and MCF10CA1a exosomes, respectively, versus PBS treatment (Fig. 2C). Consistent with our *in vitro* findings, incubation of the Matrigel plug–exosome mixture with LCKLSL resulted in a drastic decrease in angiogenesis, as evident from Matrigel plug images (Fig. 2B). Hemoglobin content analysis from MCF10CA1a exosome-treated homogenized Matrigel plugs confirmed these results, showing an approximately 5-fold decrease with LCKLSL treatment, which did not occur with LGKLSL or exosome treatment alone (Fig. 2D); injection of Matrigel with MCF10A or MCF10AT exosomes plus LCKLSL had similar effects (Supplementary Fig. S2E and S2F). H&E staining (Supplementary Fig. S4A and S4B) and DAB (3, 3'-diaminobenzidine) immunostaining (Supplementary Fig. S4C and S4D) of Matrigel plug sections against endothelial marker CD31 (recruitment of $CD31^+$ endothelial cells indicates increased angiogenesis) confirmed our findings, showing less $CD31^+$ endothelial cells in all LCKLSL treatments than in all LGKLSL treatments (Supplementary Fig. S4A–S4D). Furthermore, LCKLSL treatment markedly reduced the number of blood vessels in the plugs, compared with LGKLSL treatment. We also reconfirmed our findings by knocking down Anx II levels in the exosomes in a different breast cancer cell line, MDA-MB-231. *In vitro* endothelial tube formation assays and *in vivo* Matrigel plug assays were performed with exosomes after knocking down Anx II (231-Anx IIKD-Exo) and compared with control (231-Control-Exo). Quantification of the *in vitro* angiogenesis assay showed that 231-Anx IIKD-Exo treatment generated approximately 4.5- and 3-fold decrease in the number of meshes per field and number of branch points per field, respectively, compared with 231-Control-Exo treatment (Supplementary Fig. S3A and S3B). The Matrigel plug assay with 231-Anx IIKD-Exo treatment also revealed approximately 5-fold less hemoglobin content on average per Matrigel than 231-Control-Exo treatment (Supplementary Fig. S3C and S3D).

Exo-Anx II promotes angiogenesis in a tPA-dependent manner

To investigate the molecular mechanism by which exo-Anx II promotes angiogenesis, we performed a detailed analysis of the affected signaling pathways. We found that antibody-mediated blocking of tPA nullified the proangiogenic effects of exo-Anx II. Incubation of tPA antibody-pretreated HUVECs with 231-Control-Exo showed an approximately 2.6-fold decrease in the number of meshes per field than did IgG control treatment (Fig. 3A and B). Similarly, the number of branch points per field decreased approximately 2.75-fold after tPA antibody pretreatment, compared with IgG control (Fig. 3C). These results indicate that similar to cell surface Anx II, exo-Anx II also mediates its proangiogenic effects via tPA, probably by acting as a receptor for both tPA and plasminogen (14, 15, 28).

Exo-Anx II promotes breast cancer metastasis to lungs

Although MCF10CA1a is a highly metastatic cell line, MDA-MB-231 and its organ-specific metastatic variants, MDA-MB-831 (brain metastatic) and MDA-MB-4175 (lung metastatic), are very well characterized for organ-specific metastatic studies (29–31). Thus, for our metastatic studies, we used MDA-MB-231, MDA-MB-831, and MDA-MB-4175 cells. We found that intravenous (tail vein) exosome injection led to organotropism of the breast cancer exosomes, as fluorescently tagged MDA-MB-4175 lung metastatic exosomes showed approximately 5.5-fold more lung localization than MDA-MB-231 or MDA-MB-831 exosomes (Supplementary Fig. S5B and S5C); this indicates possible mechanistic cross-talk between the exosomes and the homing organ, leading to organotropism.

For our organ-specific metastatic studies, we knocked down Anx II by shRNA in MDA-MB-231, MDA-MB-831, and MDA-MB-4175 cells. Western blotting of the WCLs (Fig. 3D) and the exosomal lysates (Fig. 3E) showed the levels of Anx II in the specific fractions. Quantification is shown in Fig. 3F; exosome designations for all the groups are given in Supplementary Fig. S3E).

First, we tested the lung metastasis model by lateral tail vein injection. Challenge with 2×10^6 luciferase-positive MDA-MB-231-luc cells (tail vein) after one month of exosome priming showed increased lung metastasis in 231-Control-Exo–primed animals compared with 231-Anx IIKD-Exo–primed (∼2-fold) or PBS-treated animals (∼6-fold; Fig. 3G). Quantification of the number of metastatic lung nodules showed that priming with 231-Control-Exo resulted in approximately 12- and 2.5-fold increases in the number of nodules, compared with PBS-primed and 231-Anx IIKD-Exo–primed animals, respectively (Fig. 3I and J). We confirmed our results with H&E staining and human vimentin immunostaining of the lung sections, which showed significant metastasis, having larger metastatic lung nodules in 231-Control-Exo–primed animals than 231-Anx IIKD-Exo–primed animals, which had much smaller metastatic nodules (Fig. 4A and B).

We further studied the role of exo-Anx II in lung metastasis in a different metastatic model, intracardiac injection metastatic model. Challenge with 1×10^5 luciferase-positive MDA-MB-4175-luc cells after one month of exosome priming showed greater lung metastasis in 4175-Control-Exo–primed animals than in 4175-Anx IIKD-Exo–primed animals (∼1.8-fold) or PBS-treated animals (∼2.4-fold; Fig. 3H). Quantification of the number of metastatic lung nodules showed that priming with 4175-Control-Exo resulted in approximately 8- and 2-fold more nodules than PBS- and 4175-Anx IIKD-Exo–primed animals, respectively (Fig. 3K), similar to our MDA-MB-231-luc results, further confirming the important role of exo-Anx II in lung metastasis. These data clearly show that exo-Anx II promotes breast cancer metastasis to the lungs.

Exo-Anx II promotes breast cancer metastasis to brain

To study whether exo-Anx II promotes brain metastasis, we utilized two different experimental setups. First, we primed the animals with PBS, 831-Anx IIKD-Exo, or 831-Control-Exo and then challenged them with 1×10^5 MDA-MB-231-luc cells (intracardially). BLI of the animals revealed significant differences among the different treatment groups: Animals primed with 831-Control-Exo showed increased brain metastasis when compared with 831-Anx IIKD-Exo–primed animals (∼2-fold) or PBS-treated animals (∼3.8-fold; Fig. 4C).

Next, we injected 1×10^5 MDA-MB-831-luc cells (intracardially) in PBS-, 831-Anx IIKD-Exo-, or 831-Control-Exo–primed animals. Similar to our MDA-MB-231-luc findings, we saw significant differences among the different treatment groups, but the differences were more pronounced than in the MDA-MB-231-luc–challenged animals. Animals primed with 831-Control-Exo showed significantly higher brain metastasis

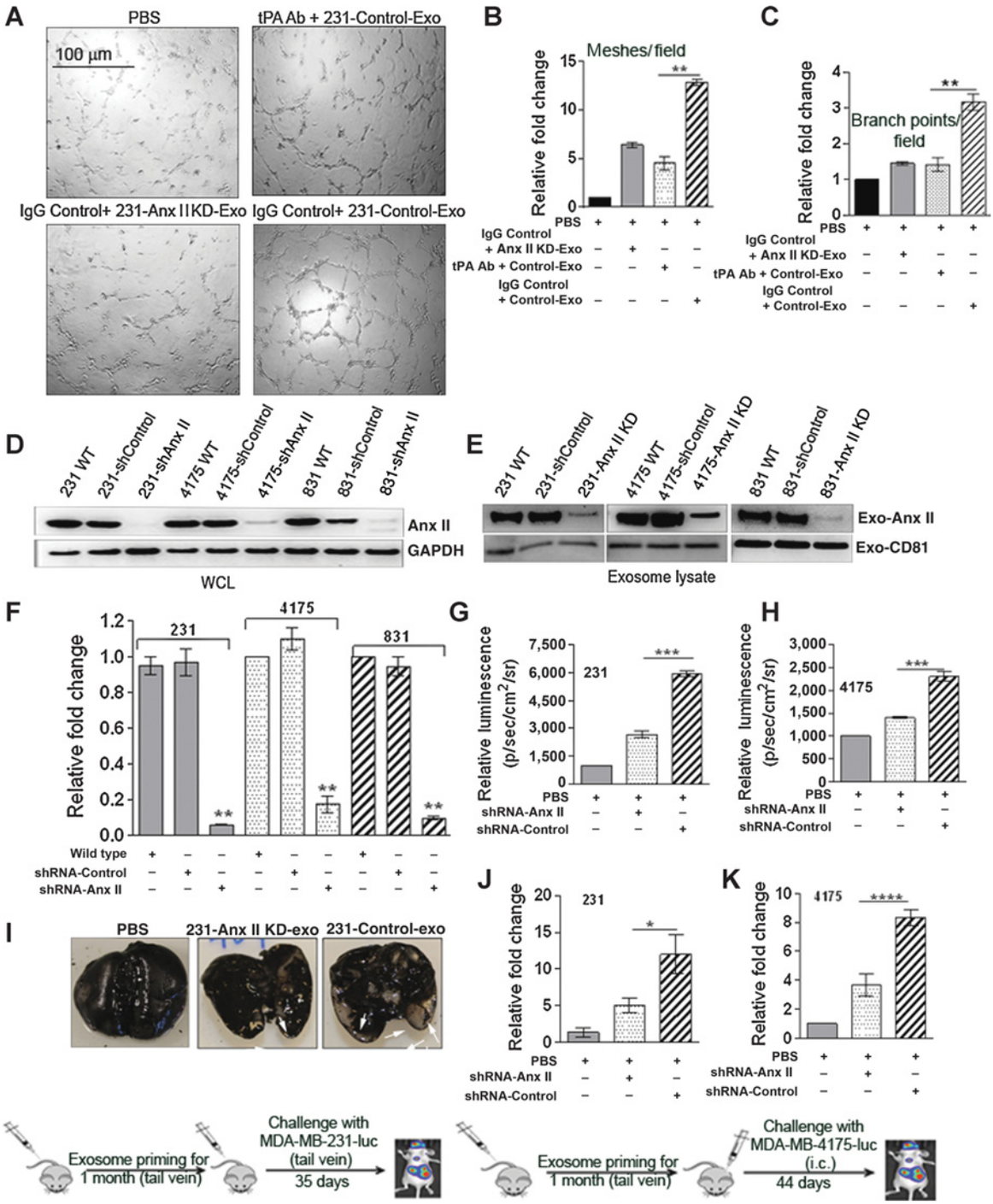

Figure 3.

Exo-Anx II promotes angiogenesis via tPA and activates macrophages, leading to secretion of IL6 and TNFα. **A,** Endothelial tube formation assay showing the role of tPA in the proangiogenic effect of exo-Anx II ($n = 2$). **B** and **C,** Quantification of the number of meshes/field (**B**) and number of branch points/field (**C**). Exo-Anx II promotes breast cancer metastasis to lungs. **D** and **E,** Western blot analysis of WCL (**D**) and exosomal lysates (**E**) showing knockdown of Anx II ($n = 2$); GAPDH and CD81 were used as loading controls for (**D**) and (**E**), respectively. **F,** Quantification of exosomal Anx II. **G,** Quantification of BLI of PBS-, 231-Anx IIKD-Exo-, or 231-Control-Exo–primed animals 35 days after challenge with MDA-MB-231-luc cells (lateral tail vein injection), showing differences in the extent of lung metastasis ($n = 8$). Fold change in photon flux to PBS-primed animals is shown. **H,** Quantification of BLI of PBS-, 4175-Anx IIKD-Exo-, or 4175-Control-Exo–primed animals 44 days after challenge with MDA-MB-4175-luc cells (intracardiac; i.c.) showing differences in the extent of lung metastasis ($n = 8$). Fold change in photon flux to PBS-primed animals is shown. **I,** India ink staining of the excised lungs from MDA-MB-231-luc cell–injected animals, showing the number of metastatic nodules. **J** and **K,** Quantification of the number of metastatic lung nodules with MDA-MB-231-luc (tail vein injection) treatment (**J**) and MDA-MB-4175-luc (intracardiac) treatment (**K**). Fold change compared with PBS-primed animals is shown. *, $P < 0.05$; **, $P < 0.01$; ***, $P < 0.001$; ****, $P < 0.0001$.

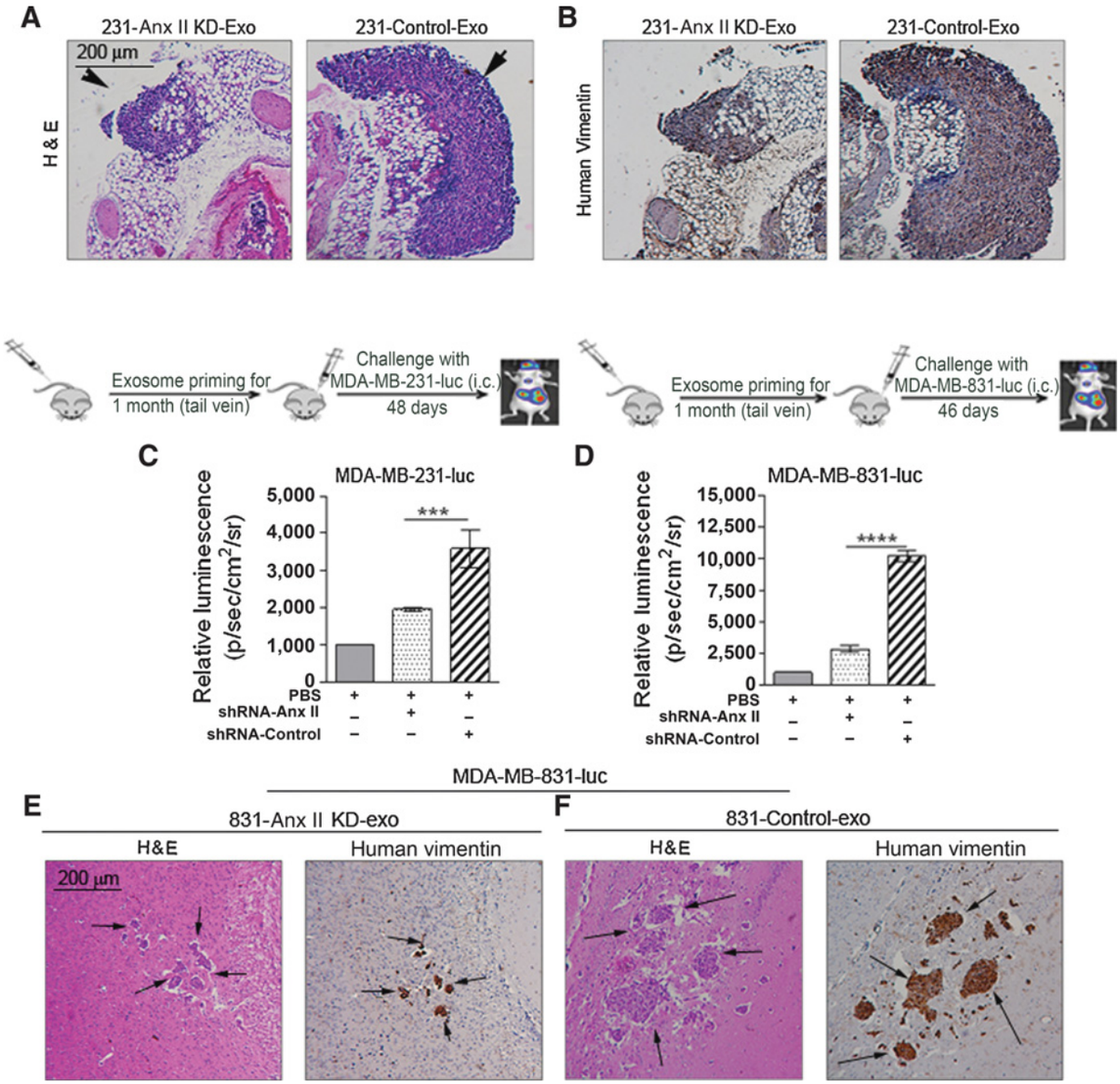

Figure 4.

A, Representative images of H&E staining and DAB immunostaining of the lung sections against human vimentin, showing the localized areas of lung metastasis ($n = 2$). Arrowheads, metastatic lung nodules. Scale bar, 200 μm. All the H&E and DAB images were captured using a Nikon phase-contrast microscope attached to a Canon camera. Exo-Anx II promotes breast cancer metastasis to brain. **C** and **D,** BLI quantification in MDA-MB-231-luc–challenged (**C**) and MDA-MB-831-luc–challenged (**D**) animals. Fold change in photon flux compared with PBS-primed animals is shown. **E** and **F,** Representative images of H&E staining and DAB immunostaining of the brain sections against human vimentin, showing the localized areas of brain metastasis ($n = 2$). Scale bar, 200 μm. All the H&E and DAB images were captured using a Nikon phase-contrast microscope attached to a Canon camera. ***, $P < 0.001$; ****, $P < 0.0001$.

than 831-Anx IIKD-Exo–primed animals (~4-fold) or PBS-treated animals (~10-fold; Fig. 4D). We confirmed our results with H&E staining and human vimentin immunostaining of the brain sections, which showed significant macrometastasis in 831-Control-Exo–primed animals, whereas 831-Anx IIKD-Exo–primed animals showed micrometastasis (Fig. 4E and F). In both of these brain metastatic studies, we found that exosome priming increased brain metastasis. Interestingly, in MDA-MB-231-luc–injected animals, PBS priming showed whole-body distribution of the cells, whereas 831-Exo priming led to greater localization of the cancer cells to the brain.

Furthermore, in both lung and brain metastatic models, we discovered that the respective exosome treatments led to a higher rate of organ-specific metastasis (photon flux vs. time) in Control-Exo–primed animals (high BLI, starting from 2 weeks) than their Anx IIKD-Exo counterparts, suggesting that exo-Anx II priming creates a microenvironment that leads to faster and higher brain and lung metastases (Fig. 5A and B).

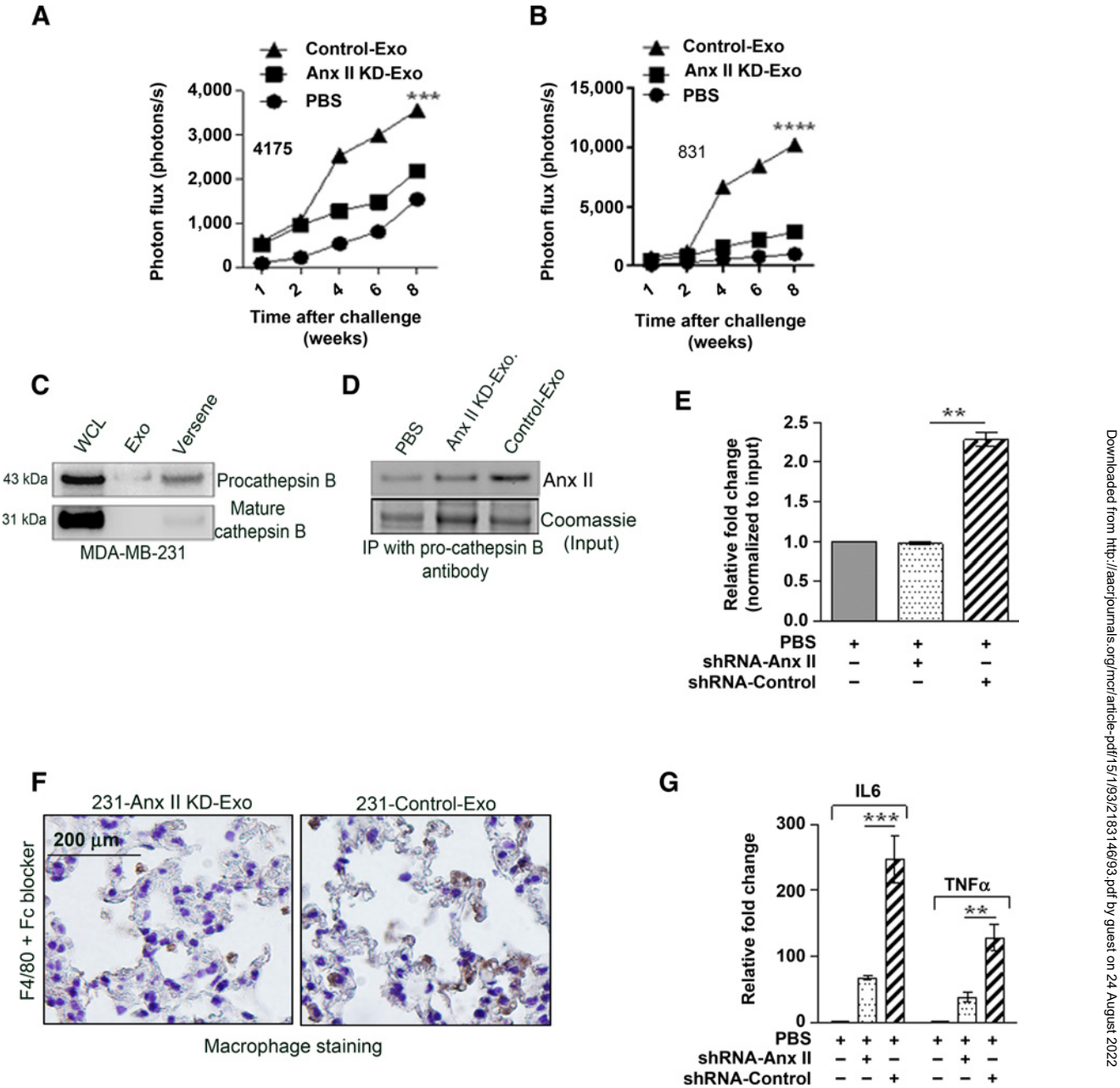

Figure 5.

Quantification of photon flux change over time: **A** and **B,** MDA-MB-4175-luc–injected lung metastasis and MDA-MB-831-luc–injected brain metastasis (**B**). **C,** Western blot analysis showing the expression of pro-cathepsin B and mature cathepsin B in WCL, Exo lysate, and membrane wash (Versene) fractions. **D,** Immunoprecipitation of Anx II with pro-cathepsin B antibody in the membrane wash lysate after treatment with PBS, Anx IIKD-Exo, or Control-Exo. **E,** Densitometric analysis of the blot ($n = 2$). *, $P < 0.05$; **, $P < 0.01$; ***, $P < 0.001$; ****, $P < 0.0001$. **F,** DAB immunostaining of macrophages in the lung sections with F4/80 antibodies in 231-Anx IIKD-Exo- and 231-Control-Exo–primed animals after Fc blocking. Scale bar, 100 μm. **G,** ELISA of lung extracts to analyze IL6 and TNFα levels from PBS-, 231-Anx IIKD-Exo-, and 231-Control-Exo–primed animals, 24 hours after injection ($n = 2$). **, $P < 0.01$; ***, $P < 0.001$; ****, $P < 0.0001$.

Exo-Anx II creates a premetastatic niche via activation of p38, NF-κB, and STAT 3 pathways

Upon investigating the mechanism by which exo-Anx II promotes metastasis, we found that it colocalizes with pro-cathepsin B on the cell surface (Fig. 5C–E). Immunoprecipitation with cathepsin antibody in 231-Anx IIKD-Exo and 231-Control-Exo–treated 231-Anx IIKD cells showed higher pull-down (~2.25 fold) of Anx II in the latter, indicating that increased exo-Anx II treatment can lead to an increased colocalization with pro-cathepsin B.

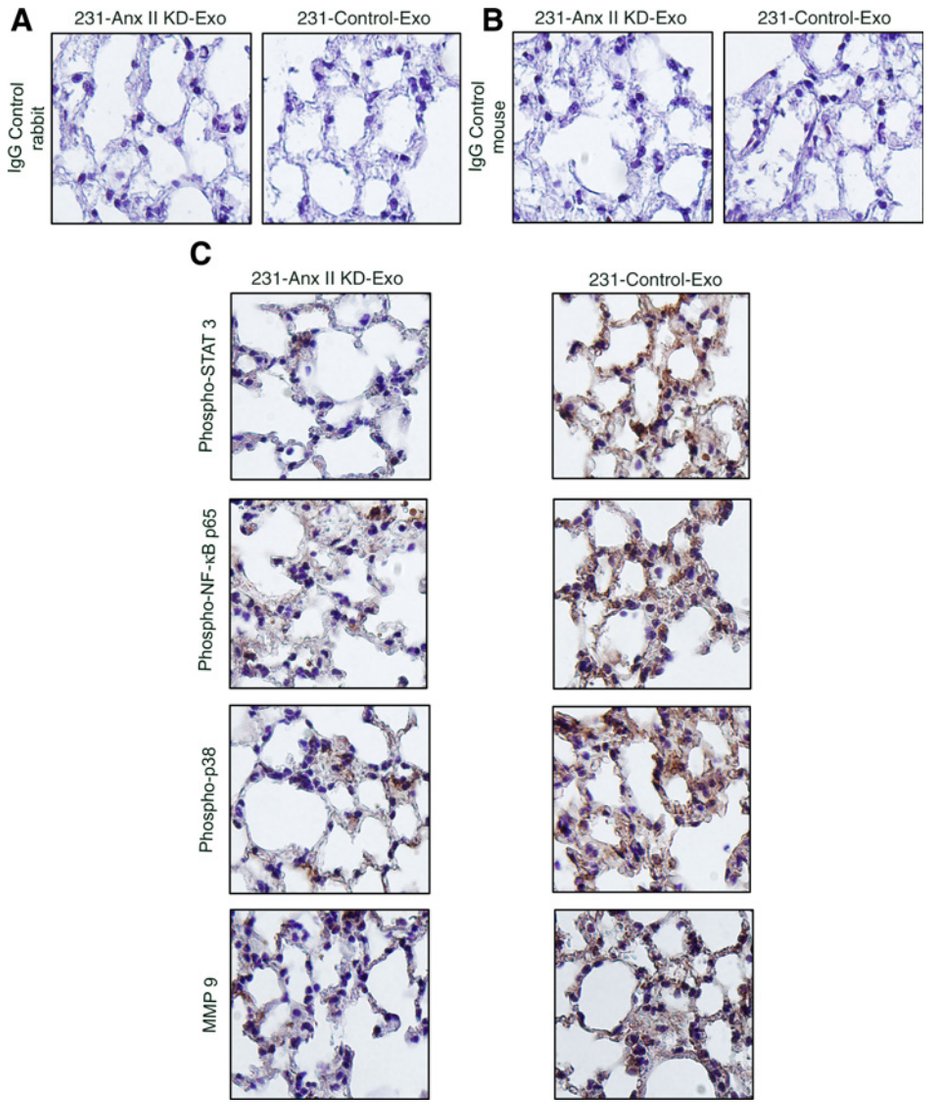

Figure 6.
Exo-Anx II activates p38-NF-κB and STAT3 signaling pathways. Immunohistochemical analysis of lung sections from 231-Anx IIKD-Exo- and 231-Control-Exo–primed animals. Representative images of DAB immunostaining for the respective proteins are shown. Scale bar, 200 μm. *, $P < 0.05$; **, $P < 0.01$; ***, $P < 0.001$; ****, $P < 0.0001$.

Previously, Swisher and colleagues have shown that secreted Anx II can activate macrophages for IL1, IL6, and TNFα secretion through MAPK and NF-κB–dependent pathways (32, 33). On the basis of this, we wanted to investigate whether exo-Anx II can activate macrophages, leading to the activation of proinflammatory signaling cascades. F4/80 staining of the lung tissues showed that 231-Control-Exo–primed animals had significantly greater positive staining for the activated macrophage marker than 231-Anx IIKD-Exo–primed animals, indicating that exo-Anx II priming leads to the activation of macrophages (Fig. 5F). Furthermore, ELISA quantification of the lungs 24 hours after (tail vein) exosome injection showed that secretion of both IL6 and TNFα was higher in 231-Control-Exo–primed animals (∼3.3- and 4-fold, respectively) than in 231-Anx IIKD-Exo–primed animals (Fig. 5G).

Our preliminary study in HUVECs revealed that 231-Control-Exo treatment activates NF-κB, p38, and STAT3 signaling cascades (∼2.5-, 2.2-, and 1.5-fold greater than control, respectively) but 231-Anx IIKD-Exo treatment does not (Supplementary Fig. S6B and S6C). Western blotting of lung extracts from exosome-primed animals confirmed our finding; Control-Exo–primed animals had approximately 2.1-, 2.2-, and 1.75-fold greater expression of phospho-NF-κB, phospho-p38, and phospho-STAT3, respectively, than Anx IIKD-Exo–primed animals (Supplementary Fig. S6D and S6E). To study the signaling pattern, we performed DAB immunostaining of the brain and lung sections. Sections from the 231-Control-Exo–primed animals showed higher phospho-STAT3 and phospho-p38-NF-κB immunostaining in the lung and brain stroma than 231-Anx IIKD-Exo–primed animals (Figs. 6 and 7); as reported earlier, MMP9 staining of the tissues also showed similar results. Analysis of the lung staining revealed that the expressions of phospho-STAT3 and phospho-p38-NF-κB were mostly confined to the alveolar network and interstitial air sacs, but were not in bronchial epithelial cells.

Discussion

Recent studies have delineated important roles of exosomal cargo in physiologic processes as well as various disease pathogenesis. In the current study, we characterized exo-Anx II in breast

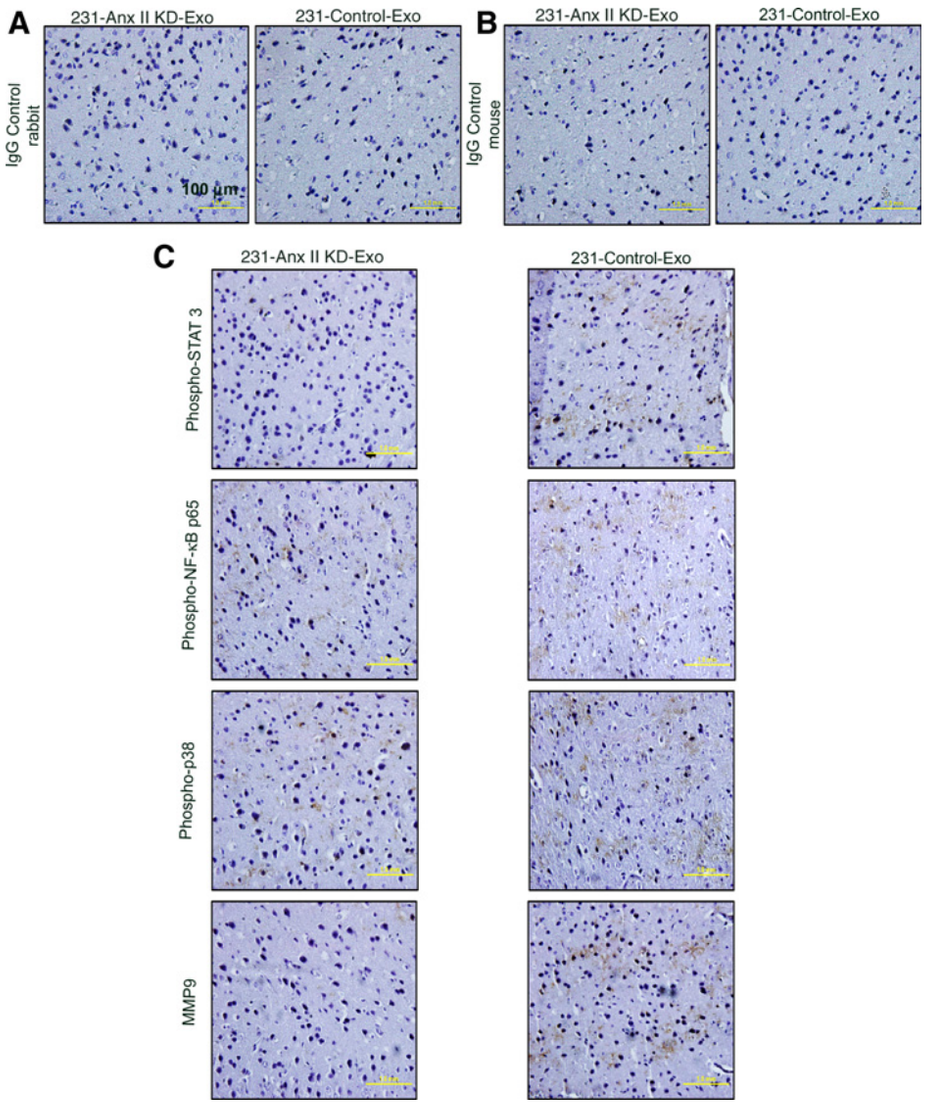

Figure 7.
Exo-Anx II activates p38-NF-κB and STAT3 signaling pathways. Immunohistochemical analysis of brain sections from 231-Anx IIKD-Exo- and 231-Control-Exo–primed animals. Representative images of DAB immunostaining for the respective proteins are shown. Scale bar, 100 μm. *, $P < 0.05$; **, $P < 0.01$; ***, $P < 0.001$; ****, $P < 0.0001$.

cancer cell lines and explored its function in promoting angiogenesis and breast cancer metastasis independently. Characterization of exo-Anx II levels in breast cancer cells revealed that highly metastatic MCF10CA1a (Fig. 1A) and MDA-MB-231 (Supplementary Fig. S1I) cells have significantly higher expression than MCF10A and MCF10AT cells. This confirms a previous finding by Jeon and colleagues, where they reported increased levels of Anx II in the media of invasive triple-negative human breast cancer cells, demonstrating a positive correlation of secreted Anx II with the invasive phenotype of breast cancer cells (13).

Anx II, along with p11 and tPA, has been reported to be a potent inducer of angiogenesis (7, 8). tPA binds to amino acid residues at positions 7–12 in the N-terminus of Anx II, corresponding to the site LCKLSL (14). Sequential mutations in the N-terminus of Anx II indicated that the cysteine residue at position 8 is crucial for the binding of tPA to Anx II; mutation of this residue significantly reduces the efficiency of tPA binding to Anx II. Previously, among an array of synthetic peptides containing cysteine residues and spanning the N-terminus of Anx II, the hexapeptide LCKLSL, which is identical in sequence to the tPA-binding site of Anx II, was >95% efficient in competitively inhibiting tPA binding to Anx II; however, replacing the cysteine residue with a glycine residue nullifies any inhibitory effect (14). In the current study, using LGKLSL control peptide and LCKLSL inhibitory peptide to specifically inhibit the function of Anx II (14, 15), we investigated whether exo-Anx II can promote angiogenesis once secreted from the cells. Utilizing various *in vitro* and *in vivo* models, we found that exo-Anx II is a potent inducer of angiogenesis and its effect can be blocked by LCKLSL inhibitory peptide. We also found that the proangiogenic effects of exo-Anx II can be attenuated by the application of tPA antibody, indicating that tPA is an important mediator of exo-Anx II–mediated angiogenesis.

Independently, we investigated the role of exo-Anx II in promoting organ-specific breast cancer metastasis. Evidence suggests that systemic factors (exosomes, microvesicles, etc.) from the primary tumor are involved in premetastatic niche formation, a specialized microenvironment that forms at the sites of future metastases and promotes the survival and outgrowth of

disseminated tumor cells (34). Using an animal model, Peinado and colleagues showed, for the first time, that melanoma exosomes educate bone marrow progenitor cells toward a prometastatic phenotype through MET (35). On the basis of this, we used a model, which, for the first time, showed that priming (regular tail vein injections of exosomes) of the animals with breast cancer exosomes can promote organ-specific breast cancer metastasis and that exo-Anx II plays a major role in this process (36). Collectively, our lung and brain metastasis data suggest that qualitative differences in exosome content can affect metastatic potential and organotropism. In addition, we found that exo-Anx II priming leads to a faster rate of organ-specific metastasis (Fig. 5A and B); however, quantification of the number of exosomes in the lungs (231 and 4,175) and brain (831) showed no significant differences between 231-Anx IIKD-Exo–primed and 231-Control-Exo–primed animals (Supplementary Fig. S6F–S6H), indicating that the differences in exo-Anx II levels were primarily responsible for the difference in the extent of metastasis. Furthermore, increased brain-specific metastasis also indicates that exosomes can cross the blood–brain barrier, as reported previously (37), and form a premetastatic niche.

Investigating the mechanism by which exo-Anx II may promote breast cancer metastasis, we found that exo-Anx II forms a premetastatic niche by activating STAT3 and p38-NFB. Swisher and colleagues previously showed that treatment of macrophages by Anx II tetramer leads to a MAPK-dependent activation of inflammatory cytokine (IL6, TNFα, and IL10) transcription by 3 hours. Interestingly, in our study, ELISA analysis of lungs tissue revealed that tail vein injection of exo-Anx II leads to the activation of IL6 and TNFα 24 hours after injection. We believe these secreted cytokines from macrophages promote tumor progression and metastasis, as reported in pancreatic cancer (38) and hepatoma (39). Similar results were obtained with 831-Control-Exo- and 4175-Control-Exo–primed animals (data not shown).

In addition, priming with 231-Control-Exo also showed increased levels of VEGFR1 in both lung and brain sections, compared with PBS-primed animals (Supplementary Fig. S5D), indicating that cancer exosomes can upregulate VEGFR1 expression, which has been previously linked with breast cancer metastasis (40, 41).

We also discovered that exo-Anx II priming leads to increased MMP9 expression in the tissues (Figs. 6 and 7), possibly further contributing to extracellular proteolysis and angiogenesis.

There is also a possibility that in addition to creating a premetastatic niche, exo-Anx II secreted by cancer cells can participate in autocrine and paracrine signaling, acting on the cancer cells themselves and promoting migration, invasion, and metastasis. A preliminary analysis of the effect of exo-Anx II on 231-Anx IIKD breast cancer cells shows that, once taken up, exo-Anx II colocalizes with pro-cathepsin B on the cell surface (Fig. 5C–E). Western blotting of the IP lysates showed much greater Anx II pull-down in 231-Control-Exo–treated cells than 231-Anx IIKD-Exo–treated cells. Previously, we have shown that exo-Anx II is internalized and can be recycled to be expressed on the cell surface (15); we believe that internalized exo-Anx II probably exists in a complex with pro-cathepsin B, tPA, plasminogen, and p11, as reported earlier (42), and helps in ECM degradation, plasmin generation, and metastatic dissemination of the breast cancer cells. However, further studies are needed to delineate the detailed mechanism by which exo-Anx II promotes breast cancer metastasis.

Although we were able to achieve significant knockdown of Anx II in our cells and exosomes, we were not able to completely remove Anx II from our treatments. Thus, one of the major drawbacks of this study is the observed effects due to residual Anx II in KD treatments. We tried to address this problem by using multiple controls. However, better experimental models, such as using gene editing techniques (CRISPR, TALEN), to completely remove Anx II- or Anx II-null mouse models are needed to clearly delineate the effects of exo-Anx II.

In conclusion, our data show that exo-Anx II is an important component of the breast cancer–microenvironment signaling. It promotes angiogenesis and vascularization by tPA-dependent increase in plasmin generation. Independent of its angiogenesis function, we found that exo-Anx II also leads to the activation of macrophage, creating a premetastatic aiding in distant organ-specific breast cancer metastasis.

Disclosure of Potential Conflicts of Interest

No potential conflicts of interest were disclosed.

Authors' Contributions

Conception and design: S. Maji, P. Chaudhary, J.K. Vishwanatha
Development of methodology: S. Maji, J.K. Vishwanatha
Acquisition of data (provided animals, acquired and managed patients, provided facilities, etc.): S. Maji, I. Akopova
Analysis and interpretation of data (e.g., statistical analysis, biostatistics, computational analysis): S. Maji, P. Chaudhary, I. Akopova, R.J. Hare
Writing, review, and/or revision of the manuscript: S. Maji, P. Chaudhary, I. Gryczynski, J.K. Vishwanatha
Administrative, technical, or material support (i.e., reporting or organizing data, constructing databases): P.M. Nguyen, J.K. Vishwanatha
Study supervision: J.K. Vishwanatha

Acknowledgments

The authors would like to thank the UNTHSC Microscopy Core Facility, Dr. A. Brun, I. Chang (for technical help), Dr. Sanjay Thamake, and Dr. Mallika Valapala (for valuable experimental input).

Grant Support

This work was supported by National Institute on Minority Health and Health Disparities grant 1P20 MD006882 (to J.K. Vishwanatha).

The costs of publication of this article were defrayed in part by the payment of page charges. This article must therefore be hereby marked *advertisement* in accordance with 18 U.S.C. Section 1734 solely to indicate this fact.

Received May 9, 2016; revised September 5, 2016; accepted October 3, 2016; published OnlineFirst October 19, 2016.

References

1. Grange C, Tapparo M, Collino F, Vitillo L, Damasco C, Deregibus MC, et al. Microvesicles released from human renal cancer stem cells stimulate angiogenesis and formation of lung premetastatic niche. Cancer Res 2011;71:5346–56.
2. Castellana D, Zobairi F, Martinez MC, Panaro MA, Mitolo V, Freyssinet JM, et al. Membrane microvesicles as actors in the establishment of a favorable prostatic tumoral niche: a role for activated fibroblasts and CX3CL1-CX3CR1 axis. Cancer Res 2009;69:785–93.

3. Wysoczynski M, Ratajczak MZ. Lung cancer secreted microvesicles: underappreciated modulators of microenvironment in expanding tumors. Int J Cancer 2009;125:1595–603.
4. Peinado H, Lavotshkin S, Lyden D. The secreted factors responsible for pre-metastatic niche formation: old sayings and new thoughts. Semin Cancer Biol 2011;21:139–46.
5. Yang C, Robbins PD. The roles of tumor-derived exosomes in cancer pathogenesis. Clin Dev Immunol 2011;2011:842849.
6. Rescher U, Ludwig C, Konietzko V, Kharitonenkov A, Gerke V. Tyrosine phosphorylation of annexin A2 regulates Rho-mediated actin rearrangement and cell adhesion. J Cell Sci 2008;121:2177–85.
7. Lokman NA, Ween MP, Oehler MK, Ricciardelli C. The role of annexin A2 in tumorigenesis and cancer progression. Cancer Microenviron 2011;4:199–208.
8. Hajjar KA, Acharya SS. Annexin II and regulation of cell surface fibrinolysis. Ann N Y Acad Sci 2000;902:265–71.
9. Wang J, Betancourt AM, Mobley JA, Lamartiniere CA. Proteomic discovery of genistein action in the rat mammary gland. J Proteome Res 2011; 10:1621–31.
10. Ling Q, Jacovina AT, Deora A, Febbraio M, Simantov R, Silverstein RL, et al. Annexin II regulates fibrin homeostasis and neoangiogenesis *in vivo*. J Clin Invest 2004;113:38–48.
11. Valapala M, Vishwanatha JK. Lipid raft endocytosis and exosomal transport facilitate extracellular trafficking of annexin A2. J Biol Chem 2011; 286:30911–25.
12. Simpson RJ, Kalra H, Mathivanan S. ExoCarta as a resource for exosomal research. J Extracell Vesicles 2012;1.
13. Jeon YR, Kim SY, Lee EJ, Kim YN, Noh DY, Park SY, et al. Identification of annexin II as a novel secretory biomarker for breast cancer. Proteomics 2013;13:3145–56.
14. Roda O, Valero ML, Peiro S, Andreu D, Real FX, Navarro P. New insights into the tPA-annexin A2 interaction. Is annexin A2 CYS8 the sole requirement for this association? J Biol Chem 2003;278:5702–9.
15. Valapala M, Thamake SI, Vishwanatha JK. A competitive hexapeptide inhibitor of annexin A2 prevents hypoxia-induced angiogenic events. J Cell Sci 2011;124:1453–64.
16. Lee GY, Kenny PA, Lee EH, Bissell MJ. Three-dimensional culture models of normal and malignant breast epithelial cells. Nat Methods 2007;4:359–65.
17. Tavazoie SF, Alarcon C, Oskarsson T, Padua D, Wang Q, Bos PD, et al. Endogenous human microRNAs that suppress breast cancer metastasis. Nature 2008;451:147–52.
18. Lasser C, Eldh M, Lotvall J. Isolation and characterization of RNA-containing exosomes. J Vis Exp 2012:e3037.
19. Franzen CA, Simms PE, Van Huis AF, Foreman KE, Kuo PC, Gupta GN. Characterization of uptake and internalization of exosomes by bladder cancer cells. BioMed Res Int 2014;2014:619829.
20. Sharma S, Rasool HI, Palanisamy V, Mathisen C, Schmidt M, Wong DT, et al. Structural-mechanical characterization of nanoparticle exosomes in human saliva, using correlative AFM, FESEM, and force spectroscopy. ACS Nano 2010;4:1921–6.
21. Merchan JR, Kovacs K, Railsback JW, Kurtoglu M, Jing Y, Pina Y, et al. Antiangiogenic activity of 2-deoxy-D-glucose. PLoS One 2010;5:e13699.
22. Drabkin DL, Austin JH. Spectrophotometric studies. II. Preparation from washed blood cells; nitric oxide hemoglobin and sulfhemoglobin. J Biol Chem 1935;112:51–65.
23. Mineo M, Garfield SH, Taverna S, Flugy A, De Leo G, Alessandro R, et al. Exosomes released by K562 chronic myeloid leukemia cells promote angiogenesis in a Src-dependent fashion. Angiogenesis 2012;15:33–45.
24. Liang Z, Yoon Y, Votaw J, Goodman MM, Williams L, Shim H. Silencing of CXCR4 blocks breast cancer metastasis. Cancer Res 2005;65:967–71.
25. Adiseshaiah PP, Patel NL, Ileva LV, Kalen JD, Haines DC, McNeil SE. Longitudinal imaging of cancer cell metastases in two preclinical models: a correlation of noninvasive imaging to histopathology. Int J Mol Imaging 2014;2014:102702.
26. Jenkins DE, Hornig YS, Oei Y, Dusich J, Purchio T. Bioluminescent human breast cancer cell lines that permit rapid and sensitive *in vivo* detection of mammary tumors and multiple metastases in immune deficient mice. Breast Cancer Res 2005;7:R444–54.
27. Kadota M, Yang HH, Gomez B, Sato M, Clifford RJ, Meerzaman D, et al. Delineating genetic alterations for tumor progression in the MCF10A series of breast cancer cell lines. PLoS One 2010;5:e9201.
28. Kumar R, Yoneda J, Bucana CD, Fidler IJ. Regulation of distinct steps of angiogenesis by different angiogenic molecules. Int J Oncol 1998; 12:749–57.
29. Selicharova I, Sanda M, Mladkova J, Ohri SS, Vashishta A, Fusek M, et al. 2-DE analysis of breast cancer cell lines 1833 and 4175 with distinct metastatic organ-specific potentials: comparison with parental cell line MDA-MB-231. Oncol Rep 2008;19:1237–44.
30. Barney LE, Dandley EC, Jansen LE, Reich NG, Mercurio AM, Peyton SR. A cell-ECM screening method to predict breast cancer metastasis. Integr Biol 2015;7:198–212.
31. Png KJ, Yoshida M, Zhang XH, Shu W, Lee H, Rimner A, et al. MicroRNA-335 inhibits tumor reinitiation and is silenced through genetic and epigenetic mechanisms in human breast cancer. Genes Dev 2011;25: 226–31.
32. Swisher JF, Burton N, Bacot SM, Vogel SN, Feldman GM. Annexin A2 tetramer activates human and murine macrophages through TLR4. Blood 2010;115:549–58.
33. Swisher JF, Khatri U, Feldman GM. Annexin A2 is a soluble mediator of macrophage activation. J Leukoc Biol 2007;82:1174–84.
34. Alderton GK. Metastasis. Exosomes drive premetastatic niche formation. Nat Rev Cancer 2012;12:447.
35. Peinado H, Aleckovic M, Lavotshkin S, Matei I, Costa-Silva B, Moreno-Bueno G, et al. Melanoma exosomes educate bone marrow progenitor cells toward a pro-metastatic phenotype through MET. Nat Med 2012; 18:883–91.
36. Wang CY, Lin CF. Annexin A2: its molecular regulation and cellular expression in cancer development. Dis Markers 2014;2014: 308976.
37. Alvarez-Erviti L, Seow Y, Schapira AH, Gardiner C, Sargent IL, Wood MJ, et al. Lysosomal dysfunction increases exosome-mediated alpha-synuclein release and transmission. Neurobiol Dis 2011;42:360–7.
38. Zhang Y, Yan W, Collins MA, Bednar F, Rakshit S, Zetter BR, et al. Interleukin-6 is required for pancreatic cancer progression by promoting MAPK signaling activation and oxidative stress resistance. Cancer Res 2013;73:6359–74.
39. Ohishi W, Cologne JB, Fujiwara S, Suzuki G, Hayashi T, Niwa Y, et al. Serum interleukin-6 associated with hepatocellular carcinoma risk: a nested case-control study. Int J Cancer 2014;134:154–63.
40. Duda DG, Jain RK. Premetastatic lung "niche": is vascular endothelial growth factor receptor 1 activation required? Cancer Res 2010;70:5670–3.
41. Psaila B, Kaplan RN, Port ER, Lyden D. Priming the `soil' for breast cancer metastasis: the pre-metastatic niche. Breast Dis 2006;26:65–74.
42. Roshy S, Sloane BF, Moin K. Pericellular cathepsin B and malignant progression. Cancer Metastasis Rev 2003;22:271–86.